

REPORT DOCUMENTATION PAGE

AD-A261 483



Form Approved
OMB No 0704-0188

3. Average "hour per response" including the time for reviewing instructions, searching existing data sources, gathering the collection of information, reviewing comments regarding this burden estimate or any other aspect of this collection of information, Washington Headquarters Services, Directorate for Information Operations and Reports, 1215 Jefferson Road, Management and Budget, Paperwork Reduction Project (8704-0188), Washington, DC 20503

DATE

3. REPORT TYPE AND DATES COVERED

Final Report - 01 Apr 1992 to 31 Dec 1992

4. TITLE AND SUBTITLE

3-D Analysis and Verification of Fracture Growth Mechanisms in Fiber-Reinforced Ceramic Composites

(u)

5. FUNDING NUMBERS

F49620-92-J-0220

6. AUTHOR(S)

Prof. M.P. Cleary, Dr. W.D. Keat,
Dr. M.C. Larson, F.T. Patterson

AFOSR-TR-93-0082

7. PERFORMING ORGANIZATION NAME(S) AND ADDRESS(ES)

Massachusetts Institute of Technology
77 Massachusetts Ave.
Cambridge, MA 02139

8. PERFORMING ORGANIZATION
REPORT NUMBER

9. SPONSORING / MONITORING AGENCY NAME(S) AND ADDRESS(ES)

Air Force Office of Scientific Research (AFOSR / NA)
Building 410
Bolling AFB, DC 20332-6448

10. SPONSORING / MONITORING
AGENCY REPORT NUMBER

N/A

11. SUPPLEMENTARY NOTES

N/A

12a. DISTRIBUTION / AVAILABILITY STATEMENT

Approved for public release;
Distribution unlimited.

DTIC
SELECTED
MAR 05 1993
S B D

12b. DISTRIBUTION CODE

N/A

ABSTRACT (Maximum 200 words)

This final report documents a 3-D computational and experimental investigation into the mechanics of toughening a brittle matrix by incorporating long brittle fibers. Computationally, small scale failure mechanisms ahead of a crack are explicitly modeled and merged with a continuum representation of the far field outside the process zone. Particular attention is given to the interfacial decohesion and frictional slipping near the tip of a matrix crack which is impinging upon an inclusion. The surface integral and finite element (SIFEH) method, which employs the principle of superposition to combine the best features of two powerful numerical techniques, provides an extremely flexible and efficient computational platform for modeling linear elastic fractures near material inhomogeneities. Applications to general 3-D fracture growth in multimaterial media demonstrate the capabilities of the computational technique and are also described. The computational simulation is being guided by laboratory experiments. Crack growth observations made on a model (micro-) structure comprising a glass rod embedded in a cement matrix show the toughening mechanisms of crack pinning and crack bridging in operation. In a second experiment, interfacial slip evolution was modeled experimentally for planar bimaterial interfaces. This combined experimental and numerical program has provided insight into optimal combinations of the key parameters (e.g. residual stresses at interface, friction coefficient, strength of fibers) to maximize toughness.

14. SUBJECT TERMS

Fracture Mechanics; Fiber-Reinforced Composites;
Ceramic Composite Materials; Surface-Integral Method;

15. NUMBER OF PAGES

16. PRICE CODE

17. SECURITY CLASSIFICATION
OF REPORT

UNCLASSIFIED

18. SECURITY CLASSIFICATION
OF THIS PAGE

UNCLASSIFIED

19. SECURITY CLASSIFICATION
OF ABSTRACT

UNCLASSIFIED

20. LIMITATION OF ABSTRACT

SAR

NSN 7540-01-280-5500

93 3 4 018

Standard Form 298 (Rev 2-89)
Prescribed by ANSI Std Z39-18
298-102

93-04652



3306

Air Force Contract No. F49620-92-J-0220

**3-D ANALYSIS AND VERIFICATION OF FRACTURE GROWTH
MECHANISMS IN FIBER-REINFORCED CERAMIC COMPOSITES**

**Michael P. Cleary, Associate Professor
Department of Mechanical Engineering
Massachusetts Institute of Technology
Cambridge, MA 02139**

31 December 1992

Final Report

Prepared for:
**Air Force Office of Scientific Research
Building 410
Bolling AFB, D.C. 20332**

3-D Analysis and Verification of Fracture Growth Mechanisms in Fiber-Reinforced Ceramic Composites

Final Report

**Michael Cleary, Principal Investigator
Associate Professor
M.I.T.**

**Dr. C.I. Chang, Dr. John Botsis
Director of Aerospace Science
AFOSR**

SUMMARY

This final report documents a 3-D computational and experimental investigation into the mechanics of toughening a brittle matrix by incorporating long brittle fibers. Computationally, small scale failure mechanisms ahead of a crack are explicitly modeled and merged with a continuum representation of the far field outside the process zone. Particular attention is given to the interfacial decohesion and frictional slipping near the tip of a matrix crack which is impinging upon an inclusion. The surface integral and finite element (SIFEH) method, which employs the principle of superposition to combine the best features of two powerful numerical techniques, provides an extremely flexible and efficient computational platform for modeling linear elastic fractures near material inhomogeneities. Applications to general 3-D fracture growth in multimaterial media demonstrate the capabilities of the computational technique and are also described. The computational simulation is being guided by laboratory experiments. Crack growth observations made on a model (micro-) structure comprising a glass rod embedded in a cement matrix show the toughening mechanisms of crack pinning and crack bridging in operation. In a second experiment, interfacial slip evolution was modeled experimentally for planar bimaterial interfaces. This combined experimental and numerical program has provided insight into optimal combinations of the key parameters (e.g. residual stresses at interface, friction coefficient, strength of fibers) to maximize toughness.

This report summarizes accomplishments achieved with support of Air Force grant AFOSR-89-0005 and contract F49620-92-J-0220.

INTRODUCTION

The key episode in the fracture of a ceramic matrix/ceramic fiber composite is the interaction that takes place between an advancing crack front and the fiber-matrix interface of individual fibers. A "strong" interface will transmit high crack tip stresses inducing premature fracture of the fibers, while a "weak" interface will blunt the crack tip and allow the fracture to proceed past intact fibers. The 2-D analysis by He and Hutchinson¹ gives the design "rule of thumb" that the fracture toughness of the interface should be less than one-quarter of the toughness of the fiber to promote favorable toughening mechanisms such as bridging and pull-out. However, a completely "weak" interface will not generate the desirable friction tractions to shield the crack tip. An optimum therefore exists with regard to toughness of the material and physical properties, including interfacial bond, toughness, and friction characteristics.

Recent investigations, while providing insight to these toughening mechanisms, are restricted in their applicability by simplifying assumptions whose impact is often difficult to assess. A number of 2-D analyses have been carried out for cracks near sliding and bonding interfaces,¹⁻³ some of these in the context of fibrous inclusions.⁴⁻⁸ Axisymmetric models which account for frictional tractions on the interface have also been developed^{9,10} for the special case of a single fiber that is completely engulfed by a fracture. Other work has examined crack pinning by bonded cylindrical inclusions.^{11,12}

This summary report outlines a combined computational and experimental investigation aimed at providing a complete fracture mechanics analysis of a crack growing near a fiber and interacting with the evolving frictional sliding zone at the interface (see Figure 1). An innovative numerical scheme, the surface integral and finite element hybrid (SIFEH) method, has been developed to obtain results for cracks near and/or crossing multiple bimaterial interfaces. The basis and implementation of this technique is outlined. In addition, novel experimental tools are being employed to verify the computational solutions and are discussed. Finally, the application of these tools to the mechanisms of fracture in brittle composite materials are presented.

Accession For	
NTIS GRA&I	<input checked="checked" type="checkbox"/>
DTIC TAB	<input type="checkbox"/>
Unannounced	<input type="checkbox"/>
Justification	
By	
Distribution/	
Availability Codes	
Dist	Avail and/or
A-1	Special

DESCRIPTION OF COMPUTATIONAL APPROACH

Modeling Requirements:

Until very recently, the direct numerical modeling of the situation depicted in Figure 1 would have been viewed as impractical. The most common tool available, finite elements, was known to require an extraordinary number of degrees of freedom to capture the stress singularity along the crack periphery, a situation that was made all the more untenable by the need to globally remesh after each time step. Thus an alternate approach was sought.

In formulating the numerical procedure presented here, we have kept in mind that a suitable computational approach should not only possess sufficient generality to address the problem of Figure 1, but it should also meet the following efficiency and accuracy requirements:

Accurate Stress Intensity Factors: The difficulty in modeling a fracture lies in being able to accurately represent the singularity in stress along the continuous crack front. The accuracy is usually assessed in terms of the stress intensity factor, which serves both as a measure of the strength of the singularity and as a criterion for crack growth. It is typically desirable to maintain the error in stress intensity factor at less than a few percent because of the error amplification associated with some crack growth laws, especially in metal fatigue.

Effective Modeling of Crack Propagation: This is achieved by keeping the total number of degrees of freedom in the problem to a minimum while providing a facility for remeshing the element topology as the crack front advances. The fact that the geometry of Fig. 1 may be viewed as consisting of multiple growing fractures (i.e. the approaching main crack plus an undetermined number of slip zones on the interface) renders many of the existing numerical techniques impractical for this application.

Accurate Representation of Near-Interface Crack Tip Fields: When there remains but a narrow ligament separating an advancing fracture from a bonded bimaterial interface, the form of the singularity at the crack tip is known to deviate dramatically from the homogeneous case. As this is also reflected in the magnitude of the stress intensity factor, we can expect the interface to have pronounced effect on the fracture growth near bonded

fibers/inclusions. This class of problems is important both as a precursor to the onset of interfacial slip and to the limiting case of interfacial friction.

Surface Integral Method:

The effectiveness of the surface-integral method at modeling 3-D fractures in infinite regions is now well established.^{13,14} It is based on representing a fracture as a distribution of force multipoles (or displacement discontinuities). Superimposing the differential effects of the constituent multipoles leads to the governing integral equation below:

$$s(\bar{x}) = \int_{S_c} \bar{E} \gamma \delta(\bar{\zeta}) dA \quad (1)$$

where the scalar function s evaluated at \bar{x} can represent any one of the displacement or stress components, δ is the crack opening, \bar{E} is a material constant relating crack opening to the equivalent multipole strength, S_c is the fracture surface, and γ , also known as the fundamental solution (or influence function), defines the effect on s of a multipole of unit strength. The influence functions can be found by differentiating the relevant point force solution in accordance with a Taylor series expansion (for details see Refs. 15,16). Thus we may note that the range of problems that can be solved by this method is limited by the availability of the point force solution.

The application of Eq. (1) requires that we first establish the magnitudes of the crack openings. An approach that works well is to generate a system of equations using boundary collocation, i.e., the known traction boundary conditions are enforced on the crack surface at as many points as there are unknown nodal values of crack opening. However the resulting equations are all singular at $\bar{x}=\bar{\zeta}$ to the degree of being indeterminable. To bound the integrand, we subtract a singular function which by virtue of its being physically equivalent to a rigid-body translation, does not alter the equality. The following singular, but integrable, equation results:

$$u(\bar{x}) = \int_{S_T} \bar{E} \gamma [\delta(\bar{\zeta}) - \delta(\bar{x})] dA \quad (2)$$

where $t(\bar{x})$ refers to the tractions acting on the surface of the fracture and S_T spans the entire crack plane.

The advantages of the surface integral method may be summarized as follows. First, only the surface of the fracture has to be discretized; this considerably simplifies the process of remeshing the fracture as it grows. Second, the singularity at the crack tip does not require special treatment because its essential features are explicitly contained within the influence functions of the multipole. Third, accurate stress intensity factors can be obtained using coarse element meshes provided that a $\rho^{1/2}$ variation of crack opening is assumed in the near-tip region, where ρ is the perpendicular distance from the crack front.

Surface Integral and Finite Element Hybrid Method:

With the existing library of influence functions being quite limited, the surface integral method cannot be directly applied to the problem of a fracture near an arbitrarily shaped region of material inhomogeneity. Thus to retain with such problems the advantages of a surface integral analysis, it has been combined with the finite element method using incremental superposition. The resulting hybrid method opens up the possibility of accounting for a wide range of volume effects, including material inhomogeneities^{13,17,18}, thermal effects¹⁹, and plasticity.^{13,20}

The following derivation of the governing hybrid equations considers the case, shown in Figure 2, of a fracture which is fully embedded within a region of material inhomogeneity (referred to here as the subregion). It has been assumed that the only influence functions available for use are those for a multipole in an infinite, homogeneous region. It has further been assumed that the interface is sufficiently far away from the crack front so as not to either alter the form of the crack tip singularity or produce strong coupling at the interface, where the component methods will be joined.

A solution can be found by superimposing the results of the three models shown in Figure 2. Model I is an uncracked finite element model of the complete bounded domain. Model II is a surface integral model of the fracture in an infinite, homogeneous region. Since the results of Model II are not valid beyond the interface because of the mismatch in material properties, it is equivalently represented as a finite body being held in equilibrium

by tractions R^C . Model III is an uncracked finite element model of the subregion. It has been introduced to meet the requirement of displacement continuity at the interface. Since the component models of Figure 2 individually satisfy equilibrium and strain compatibility within the limits of their respective formulations, all that remains to define the solution is to enforce both the prescribed boundary conditions and the traction/displacement continuity across \mathfrak{I} . This is accomplished through the application of corrective tractions and displacements.

Overall traction continuity across \mathfrak{I} is obtained by cancelling the tractions on the external boundaries of the two subregion models, i.e., models II and III. This is done by calculating a pair of nodal load vectors, representing the external traction distributions on each model, and applying the negative of both vectors to the interface nodes of model I. Thus the finite element equations for model I will have the standard form but with two additional load vectors on the right-hand side:

$$[K]\{U^{FE}\} = \{R\} - \{R^C\} - \{R^{SUB}\} \quad (3)$$

where $[K]$ is the finite element stiffness matrix for model I, $\{U^{FE}\}$ is the vector of unknown finite element nodal displacements, and $\{R\}$ is the vector of prescribed nodal loads acting on model I. Defining the correction load vectors: $\{R^C\}$ is a nodal force approximation of the surface integral tractions acting on \mathfrak{I} and thus may be reexpressed in terms of crack opening displacement; $\{R^{SUB}\}$ refers to the nodal support reactions induced in model III by the imposition of nodal displacements $\{U^{SUB}\}$ on the interface:

$$\{R^C\} = [G]\{\delta\}; \quad \{R^{SUB}\} = [K^{SUB}]\{U^{SUB}\} \quad (4)$$

where $[K^{SUB}]$ is the finite element stiffness matrix for the subregion.

Displacement discontinuity across \mathfrak{I} , being already assured in model I, is enforced by requiring the interface nodes in model III to displace as the negative of displacements which are computed at the corresponding locations in model II:

$$\{U^{SUB}\} = -\{U^{SI}\} = -[L^{INT}]\{\delta\} \quad (5)$$

thus effectively cancelling the discontinuity in the displacement field introduced in model II when we truncated the surface integral domain at \mathfrak{I} .

The enforcement of traction boundary conditions at the crack surface is based on the surface integral equations of model II. Since the fracture has not been explicitly accounted for in either finite element model (i.e. I or III), these models will produce nonzero tractions, $\{T^C\}$ and $\{T^{SUB}\}$, at locations coincident with the surface of the fracture. To cancel these extraneous tractions, they are reversed in sign and applied as additional boundary conditions in the surface integral formulation:

$$[C]\{\delta\} = \{T\} - \{T^C\} - \{T^{SUB}\} \quad (6)$$

The evaluation of $\{T^C\}$ and $\{T^{SUB}\}$ is based on the equations of those finite elements in models I and III, respectively, which would contain the fracture if it was to be explicitly modeled. Since the mesh topologies of finite element models I and III are identical for the subregion, it follows that:

$$\{T^C\} = [S]\{U^{FE}\}; \quad \{T^{SUB}\} = [S]\{U^{SUB}\} \quad (7)$$

where the same $[S]$ applies to both $\{T^C\}$ and $\{T^{SUB}\}$.

The final step in this derivation is to rewrite the above expressions as a system of equations in terms of designated primary variables U^{FE} and δ . Two coupled systems of equations result when we substitute Eqs. (4) and (5) into (3), and Eqs. (7) and (5) into (6). When written in partitioned matrix form, they are expressed by:

$$\begin{bmatrix} K & G-K^{SUB}L^{INT} \\ S & C-SL^{INT} \end{bmatrix} \begin{pmatrix} U^{FE} \\ \delta \end{pmatrix} = \begin{pmatrix} R \\ T \end{pmatrix} \quad (8)$$

Thermally-induced strains can be modeled with the SIFEH formulation. Linear, isotropic thermal effects are computed as correction load vectors and superimposed on the model presented above.²¹ The resulting coupled system of equations takes the following form:

$$\begin{bmatrix} K & G-K^{SUB}L^{INT} \\ S & C-SL^{INT} \end{bmatrix} \begin{pmatrix} U^{FE} \\ \delta \end{pmatrix} = \begin{pmatrix} R+R^{TH} \\ T-T^{TH} \end{pmatrix} \quad (9)$$

where $\{R^{TH}\}$ and $\{T^{TH}\}$ represent, respectively, the loading in the finite element model and on the crack surface due to thermal effects. Both correction load vectors can be computed using the surface integral and finite element formulations.

One of the key advantages of the hybrid method is that the surface integral model of the fracture can be set up independently of the finite element model of the surrounding domain. The implication of this for crack propagation analysis is that only the fracture surface has to be remeshed as the crack advances through the fixed finite element model. This feature has facilitated the development of a fully automatic remeshing algorithm, suitable for use on remote supercomputing facilities where interactive inspection of the crack mesh may not be available. The remeshing strategy is based on first representing the crack front as a parametric cubic spline and then dividing the fracture surface which it encloses into two domains: a leading edge region where tip elements assume a $\rho^{1/2}$ variation of the crack opening, and an interior region where it suffices to employ low-order interpolation functions to capture the variation in crack opening. In the leading edge region where the shape and size of the tip element plays such a critical role in determining the accuracy of the stress intensity factors, heuristics are employed to construct the element geometries. The interior of the fracture is discretized by first dividing it into nearly convex subregions using a modified version of the algorithm proposed by Bykat²² and then triangulating each subregion in succession using a method of geometric decomposition developed by Chae.²³

DESCRIPTION OF EXPERIMENTAL INVESTIGATION:

The Resource Extraction Laboratory has developed a unique laboratory facility for the study of fracture growth near material inhomogeneity. Experimental simulation has supported and directed development of the SIFEH code. The apparatus used in this role are described in the following sections.

Crack Interaction Apparatus (CIA):

The model system is composed of 1.8 cm diameter glass rods embedded in large cement cylinders. The specimens are tested in the specially designed crack interaction apparatus (CIA) shown schematically in Figure 3. The CIA allows independent control of the axial and radial stresses exerted on the specimen during testing. By internally

pressurizing a precrack cast into the cement, a quasi-static fracture is propagated in the specimens, perpendicular to one or more rods (fibers). Brief deviations from a hydrostatic stress boundary condition leave small stairstep markings on the fracture surface, thereby recording the history of an advancing crack as it approaches and bows around the glass inclusions. Successive stages in crack development can be observed on each of the resulting halves of a ruptured specimen. By coating the glass rods prior to casting, the friction coefficients may be controlled and its impact assessed. Figure 4 shows representative crack growth patterns for high and low friction interfaces.

Interfacial properties for coated glass rods cast in cement are determined experimentally with push-out tests. Glass rods (fibers) are driven from the surrounding cylindrical specimens (in a state of hydrostatic compression) using an Instron test apparatus. Load-displacement histories are then evaluated to determine cohesion and frictional slip properties.

Interfacial Separation Experiment (ISE):

ISE simulates the growth of the slip zone on a planar interface normal to a pressurized crack. The apparatus uses transparent materials with variable crack geometries and interfacial friction coefficients to visually observe interfacial slip between the media. (see Figures 5,6) Computer mapping of measured interface displacements determines the shape and size of the evolving zone.

APPLICATIONS:

Crack Growth Near a Planar Bimaterial Interface:

The growth of a pressurized fracture toward a bonded bimaterial interface was modeled using the previously described surface integral method. The near-interface crack tip fields are accurately captured by employing the influence functions for a dipole near a planar bimaterial interface (see Figures 7,8 and Tables 1,2). These influence functions explicitly account for the presence of the interface so that only the surface of the fracture has to be discretized. To obtain the fracture shape shown in Figure 9, points along the initially circular crack front were incrementally advanced in proportion to the local values of $(K_I - K_{IC})$ with K_{IC} representing fracture toughness.

Fracture Intersecting Multiple Bimaterial Interfaces:

The surface integral formulation could not be directly applied to model a fracture intersecting two bimaterial interfaces because the corresponding influence functions were not available. Superposition of results derived with sets of bimaterial influence functions and application of appropriate correction loads allows accurate modeling of near-interface fracture behavior. Results obtained for fractures near two planar bimaterial interfaces are presented in Figures 10-14 and Table 3.

Interaction of Multiple 3-D Mixed Mode Fractures:

Toughening brittle materials with second phase brittle fibers involving tailoring microstructures, material properties, fiber spacing, interfaces, etc. to create an environment that favors the growth of smaller flaws over the continued growth of some dominant propagating flaw. Assessing the resulting pseudo-ductility involves the interaction of multiple fractures. There are relatively few solutions in the literature for mixed-mode interaction of numerous cracks. The surface integral method accurately replicates these existing solutions, but is not limited to simple geometries or loading. Figure 15 illustrates the variation in the stress intensity factor with distance between two parallel cracks. Results correlate well with the solutions in Ref. 26. Similar results are obtained for two coplanar cracks as shown in Figure 16.

Surface Cracks:

The SIFEH method has proven useful for modeling surface cracks in bounded domains. The bimaterial influence functions are combined using superposition as shown in Figure 17. The case of a semi-circular surface crack in a finite-thickness plate under uniform tension was used to test the approach. This geometry was investigated by Raju and Newman²⁷ using finite element methods and has been verified by subsequent studies. With minor refinement of the finite element mesh in the region of the surface flaw, the SIFEH method accurately represented the stress intensity factors along the crack front as shown in Figures 18 and 19. Similar results were obtained for the case of semi-elliptical surface crack geometries. The hybrid code used for these analyses can be used without modification to model near-interface cracks in bounded, bimaterial regions.

Evolution of Frictionally Constrained Interfacial Slip:

The extent to which fibers affect the cracking of a brittle matrix is determined by the interfacial characteristics; it is therefore important to include the evolution of frictional sliding at the matrix/fiber interface in the computational models. A Coulomb friction criterion is employed and the interface is treated as locally sticking or slipping. If the driving shear at the interface, τ_D , is of lower magnitude than the normal compression multiplied by a constant friction coefficient, $\mu\sigma_N$, then the shear transmitted across the crack faces is the driving shear, τ_D , and the interface is sticking. If the magnitude of driving shear exceeds the normal compression times the friction coefficient, the shear transmitted across the faces is $\mu\sigma_N$ (in the direction of τ_D) and the interface surfaces slip relative to one another. Thus, computationally, the shear traction imposed at each point on the crack faces does not exceed the magnitude of the normal traction multiplied by the friction coefficient. If the normal traction is tensile (loss of contact) there is no shear traction transmitted across the open crack. Conditional statements have been incorporated into the computational methodology to determine which of these conditions, stick, slip, or separation, prevails at each of the elements. Since we are dealing with slip zones evolving in time it is necessary to check these criteria at each time step.

Since, however, the shear at the interface is a boundary condition which depends upon the nature of the solution - specifically the normal stress - the shear magnitude and orientation lag one iteration behind the rest of the solution. This condition is expressed by:

$$\begin{aligned}\tau_F^{(t+\Delta t)} &= \tau_D^{(t)} & \text{for } (\tau_F^{(t)} \leq \mu\sigma_N^{(t)}) \\ \tau_F^{(t+\Delta t)} &= \mu\sigma_N^{(t)} & \text{for } (\tau_F^{(t)} > \mu\sigma_N^{(t)}) \\ \tau_F^{(t+\Delta t)} &= 0 & \text{for } (\sigma_N^{(t)} \leq 0)\end{aligned}\tag{10}$$

with τ_F = frictional shear, τ_D = driving shear at interface, μ = friction coefficient, σ_N = normal compressive traction (i.e. a negative value denotes interfacial tension), and specifies the time or loading increment. Correspondingly, the governing singular integral equations are cast in a form which allows the specification of the non-linear traction boundary condition induced by the frictional interface at each time-step:

Main Crack:

$$\sigma(\bar{x}) = \int_{s_s} \gamma(\bar{x}, \bar{x}_s) \delta(\bar{x}_s) dA + \int_{s_c} \gamma(\bar{x}, \bar{x}_c) \delta(\bar{x}_c) dA \quad (11)$$

Sliding Zone:

$$\sigma_N(\bar{x}) - \sigma_R(\bar{x}) = \int_{s_s} \gamma_N(\bar{x}, \bar{x}_s) \delta_s(\bar{x}_s) dA + \int_{s_c} \gamma_N(\bar{x}, \bar{x}_c) \delta(\bar{x}_c) dA \quad (12)$$

$$\tau_I(\bar{x}) - \mu \sigma_N(\bar{x}) = \int_{s_s} \gamma_T(\bar{x}, \bar{x}_s) \delta_s(\bar{x}_s) dA + \int_{s_c} \gamma_T(\bar{x}, \bar{x}_c) \delta(\bar{x}_c) dA \quad (13)$$

where \bar{x} denotes the locations of the collocation points, \bar{x}_c are the spatial coordinates of the main crack surface, S_c , \bar{x}_s are the spatial coordinates of the sliding zone surface, S_s , σ are the prescribed tractions, σ_N are the normal stresses induced by the displacements and loading of the main crack and slip zones (see Figure 1), σ_R are the initial normal stresses at the interface (e.g. from thermal mismatch at processing), δ are the opening and sliding displacements, and γ are the singular kernels.

The solution methodology satisfies specified traction and displacement boundary conditions. The interfacial sliding zone is iteratively determined within each time-step of matrix crack propagation; during each iteration any tendency for reverse sliding or frictional sticking is checked.

Matrix Fractures Interacting with Fibers:

A parametric study in two-dimensions revealed that the key parameter characterizing the impact of a nominally compressive frictional interface on matrix crack growth is the "frictional grab", $\mathcal{FG} = \mu \sigma_R / \sigma_O$. This is a measure of the cohesiveness of the interface based on the nominal, pre-existent compression, σ_R . (Refer to Figure 1.) For values of σ_R on the order of or greater than the driving stress σ_O , this nominal compression is dominant over the component of normal interfacial stress generated by the driving stress. If \mathcal{FG} is too low the interfaces offer no resistance to the crack opening near the periphery of small cracks and the fibers actually attract the matrix fracture. If \mathcal{FG} is too large the fibers will indeed tend to inhibit the progress of the fracture however the stress concentration in the fiber will be too severe rupturing the fibers. Models of a matrix crack propagating past a

fiber (a snapshot of one of these sequences is shown in Figure 20) were constructed for the purpose of moving fractures past frictional interfaces to determine the propensity for growth and also the longitudinal tension within the fibers.

Figures 21, 22, and 23 each show the successive stages of growth of a long crack front as it encounters and passes by a fiber for three values of frictional grab which span a range pertinent to potential brittle composite systems. It is clear from the preceding that larger frictional grab numbers, with the corresponding restricted local crack openings, lead to increases in effective matrix toughness. The transition for matrix toughening occurs near $\mathcal{FG}=0.01$.

As previously noted, however, the larger the frictional grab, the higher the stress concentration in the fiber, since load transfer from the matrix occurs over a shorter distance. Infinite frictional grab (a perfect bond) would imply an infinite stress concentration, i.e. a stress intensity in the fiber. The resulting increase in propensity for fiber failure puts a practical limitation on the magnitude of \mathcal{FG} . The limitation is expressed here in terms of the longitudinal tensile stresses within the fiber. During the course of the three simulations shown in the figures, this component of stress was monitored inside the fiber. In the single fiber model employed, the stresses in the fiber continue to grow without bound as the crack moves past since there is an ever decreasing area of matrix and only one fiber to assume the load being shed from the matrix. In a real composite the cracks will, of course, be of finite extent with additional fibers present to share the burden of the strain energy released by the advancing crack. Nonetheless, the stresses measured in the simulations are useful if interpreted in a relative sense. We can determine what percent increase in the severity of stress accompanies a specified enlargement of the frictional grab parameter.

From these simulations we can establish the important features of the design criterion we seek. A reference condition which facilitates comparison of the three is that point at which the main crack first encounters the fiber. As one might expect for this configuration, the maximum stress concentration in the fiber occurs at the point nearest the main crack. (It is noteworthy that the position of maximum stress concentration in the fiber follows the main crack periphery as it sweeps around the fiber. The magnitude of the concentration factor increases until the crack engulfs the fiber and then the magnitude

drops. This suggests that the probability of fiber failure peaks when the main crack has almost enveloped the fiber.)

Figure 24 plots the maximum local stress concentration of the tensile stress aligned with the fiber axis for the range of frictional grab values discussed previously. Depending upon the particular fiber, it may be more appropriate to use the stress averaged over a significant area (e.g. the fiber cross-section in the plane of the main crack) when considering the likelihood of fiber failure under an experimentally determined maximum tensile stress. An appropriate σ_0 for use in scaling the fiber failure stress would be the first matrix cracking strength of the composite. Once the horizontal line indicating fiber failure is placed on Figure 6 the useful range of FG can be ascertained and used as a guide for the manufacture and processing of tough composites.

CONCLUSIONS

Three-dimensional computational and experimental investigations have resulted in novel tools for the investigation into the toughening mechanisms due to incorporation of brittle fibers in brittle matrices. Application of the surface integral and finite element hybrid (SIFEH) method to a wide variety of fracture geometries in bimaterial media have shown the technique to be a flexible and efficient tool. Incorporation of thermally-induced strains and interfacial decohesion/frictional slip have further enhanced the capabilities of the method. When combined with experimental studies, the method developed will help brittle composite manufacturers tailor the material properties to suit material demands.

References:

- ¹Ming-Yuan He and J.w. Hutchinson, "Crack Deflection at an Interface Between Dissimilar Elastic Materials," *Int. J. Solids Struct.*, **25**[1] 1053-1067 (1989).
- ²K.Y. Lam and M.P. Cleary, "Slippage and Re-Initiation of (Hydraulic) Fractures at Frictional Interfaces," *Int. J. Numer. Anal. Meth. Geomech.*, **8**, 589-604 (1989).
- ³F.Erdogan and Askogan, "Bonded Half Planes Containing an Arbitrarily Oriented Crack," *Int. J. Solids Struct.*, **10**, 569-585 (1974).
- ⁴M.K. Kanninen, E.F. Rybicki, and W.I. Griffith, "Preliminary Development of a Fundamental Analysis Model for Crack Growth in a Fiber Reinforced Composite Material"; pp.53-69 in *Composite Materials: Testing and Design*. ASTM 617, American Society for Testing and Materials, 1976.
- ⁵F. Erdogan and G.D. Gupta, "The Inclusion Problem with a Crack Crossing the Boundary," *Int. J. Fract.*, **11**[1] 13-27 (1975).
- ⁶B. Budiansky, J.W. Hutchinson, and A.G. Evans, "Matrix Fracture in Fiber-Reinforced Ceramics," *J. Mech. Phys. Solids*, **34**[2] 167-189 (1986).
- ⁷B. Budiansky and John Amazigo, "Toughening by Aligned, Frictionally Constrained Fibers," Harvard University Report MECH-119 (Mar., 1988).
- ⁸D.B. Marshall, B.M. Cox, and A.G. Evans, "The Mechanics of Matrix Cracking in Brittle-Matrix Fiber Composites," *Acta Metall.*, **33**[11] 2013-2021 (1985).
- ⁹L.S. Sigl and A.G. Evans, "Effects of Residual Stress and Frictional Sliding on Cracking and Pull-Out in Brittle Matrix Composites," *Mech. Mater.*, **8**, 1-12 (1989).
- ¹⁰J.W. Hutchinson and H.M. Jensen, "Models of Fiber Debonding and Pullout in Brittle Composites with Friction," Harvard University Report MECH-157 (Feb., 1990).
- ¹¹A.G. Evans, "The Strength of Brittle Materials Containing Second Phase Dispersions," *Phil. Mag.*, **26**, 1327-1344 (1972).
- ¹²Nabil Fares, "Crack Fronts Trapped by Arrays of Obstacles: Numerical Solutions Based on Surface Integral Representation," Harvard University Report MECH-136 (Nov., 1988).
- ¹³W.D. Keat, B.S. Annigeri, and M.P. Cleary, "Surface Integral and Finite Element Hybrid Method for Two and Three-Dimensional Fracture Mechanics Analysis," *Int. J. Fract.*, **36**[1] 35-53 (1988).
- ¹⁴W.D. Keat, "Surface Integral and Finite Element Hybrid Method for the Analysis of Three-Dimensional Fractures," Ph.D. Thesis in the Department of Mechanical Engineering, M.I.T., April, 1989.
- ¹⁵M.P. Cleary, "Fundamental Solutions for a Fluid-Saturated Porous Solid," *Int. J. Solid Struct.*, **13**, 785-806 (1977).

¹⁶B.H.G. Brady, "A boundary Element Method for Three-Dimensional Elastic Analysis of Tabular Orebody Extraction," *19th U.S. Rock Mechanics Symposium*, 431-439 (1978).

¹⁷B.S. Annigeri, W.D. Keat, and M.P. Cleary, "Fracture Mechanics Research Using the Surface Integral and Finite Element Hybrid Method"; Proceedings of First Joint Japan/U.S. Symposium on Boundary Element Methods. University of Tokyo, Oct., 1988. Pergamon Press, New York.

¹⁸W.D. Keat and M.P. Cleary, "Analysis of 3-D Near-Interface Fractures in Bounded Heterogeneous Domains Using the Surface Integral and Finite Element Hybrid Method"; pp. 343-352 in Proceedings of International Symposium on Boundary Element Methods. United Technologies Research Center, Oct., 1989. Springer-Verlag.

¹⁹B.S. Annigeri, "Thermoelastic Fracture Analysis using the Surface Integral and Finite Element Hybrid Method"; presented at the ICES-88 Conference, Atlanta, Georgia, 1988.

²⁰B.S. Annigeri, "Surface Integral Finite Element Hybrid Method for Localized Problems in Continuum Mechanics," Sc.D. Thesis in the Department of Mechanical Engineering, M.I.T., April, 1984.

²¹R.J. Bsaibes, "Analysis of Three-Dimensional Fractures Subject to Thermal Loading," B.S. Thesis in the Department of Mechanical Engineering, M.I.T., June, 1991.

²²A.Bykat, "Automatic Generation of Triangular Grid: I-Subdivision of a General Polygon into Convex Subregions, II-Triangulation of Convex Polygons," *Int. J. for Numerical Methods in Engineering*, **10**, 1329-1342 (1976).

²³S.W. Chae, "On the Automatic Generation of Near-Optimal Meshes for Three-Dimensional Linear Elastic Analysis," Ph.D. Thesis in the Department of Mechanical Engineering, M.I.T., 1988.

²⁴Rongved, "Force Interior to One of Two Joined Semi-Infinite Solids"; pp. 1-13 in Proceedings of Second Midwestern Conf. on Solid Mech., 1955.

²⁵M.P. Cleary, "Primary Factors Governing Hydraulic Fractures in Heterogeneous Stratified Porous Formations"; presented at Energy and Petroleum Conference, Houston, November, 1978, ASME Paper No. 78-Pet-47, 1978.

²⁶Murakami, Stress Intensity Factors Handbook, Vol. 2. Pergamon Press, New York, 1987.

²⁷I.S. Raju and J.C. Newman, "Stress-intensity factors for a wide range of semi-elliptical surface cracks in finite thickness plates", *Engin. Fract. Mech.*, **11**, 817-829 (1979).

²⁸T.S. Cook and F. Erdogan, "Stresses in bonded materials with a crack perpendicular to the interface", *Int. J. Engin. Sci.*, **10**, 677-697 (1972).

²⁹F. Erdogan and V. Biricikoglu, "Two bonded half planes with a crack going through the interface", *Int. J. Engin. Sci.*, **11**, 745-766 (1973).

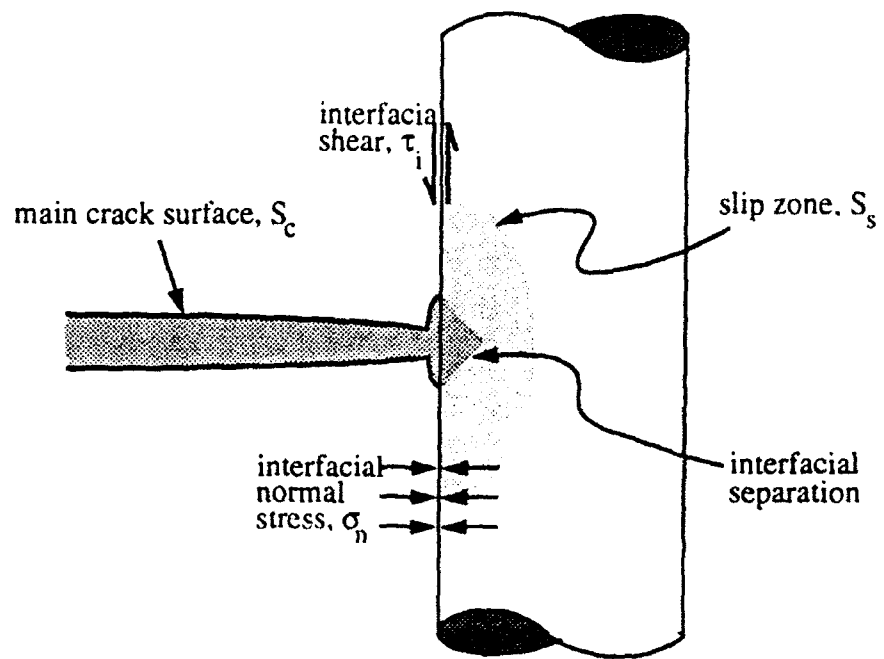


Figure 1. Physical model of a main crack impinging on a fiber-matrix frictional interface.

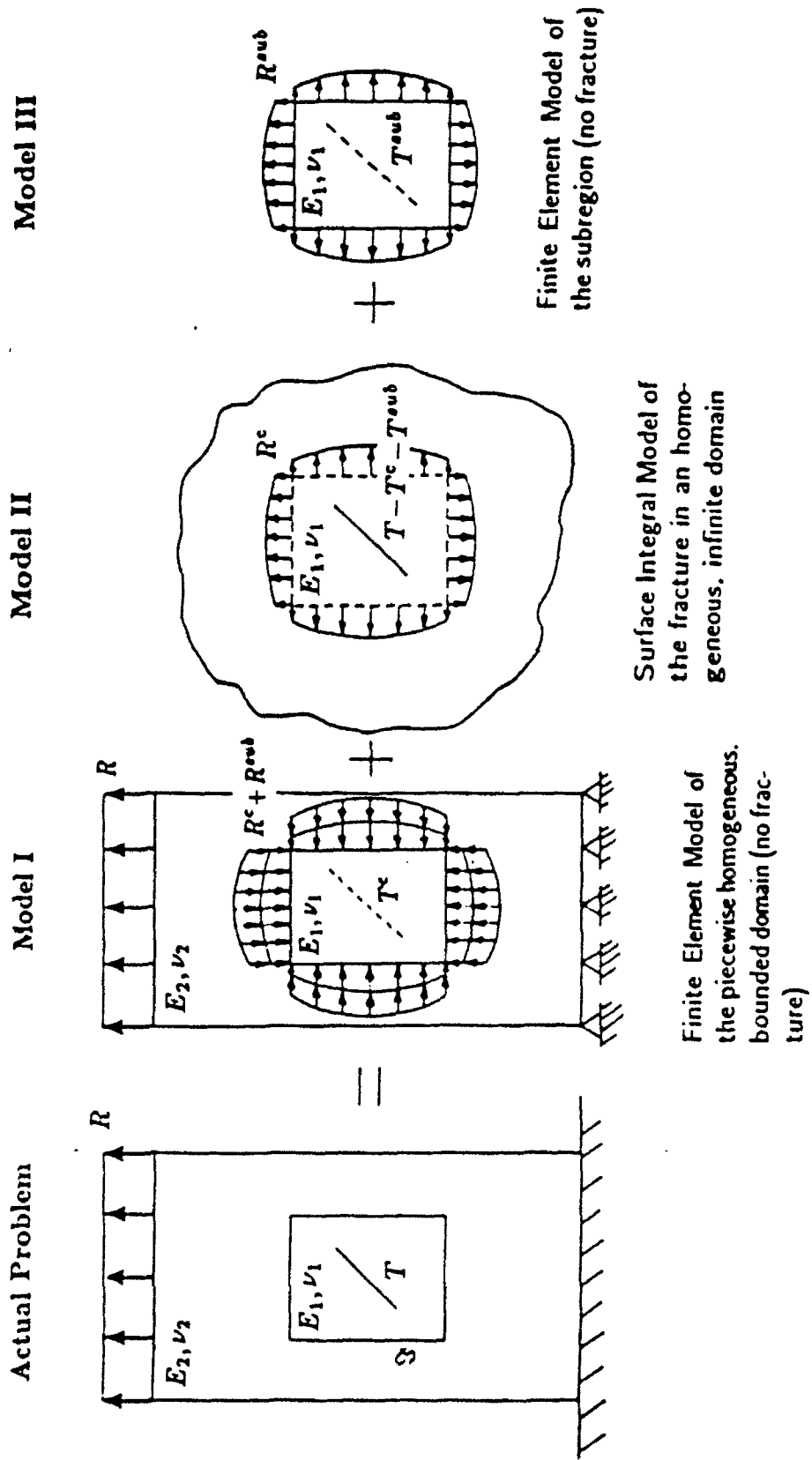


Figure 2. Component models used with subregioning.

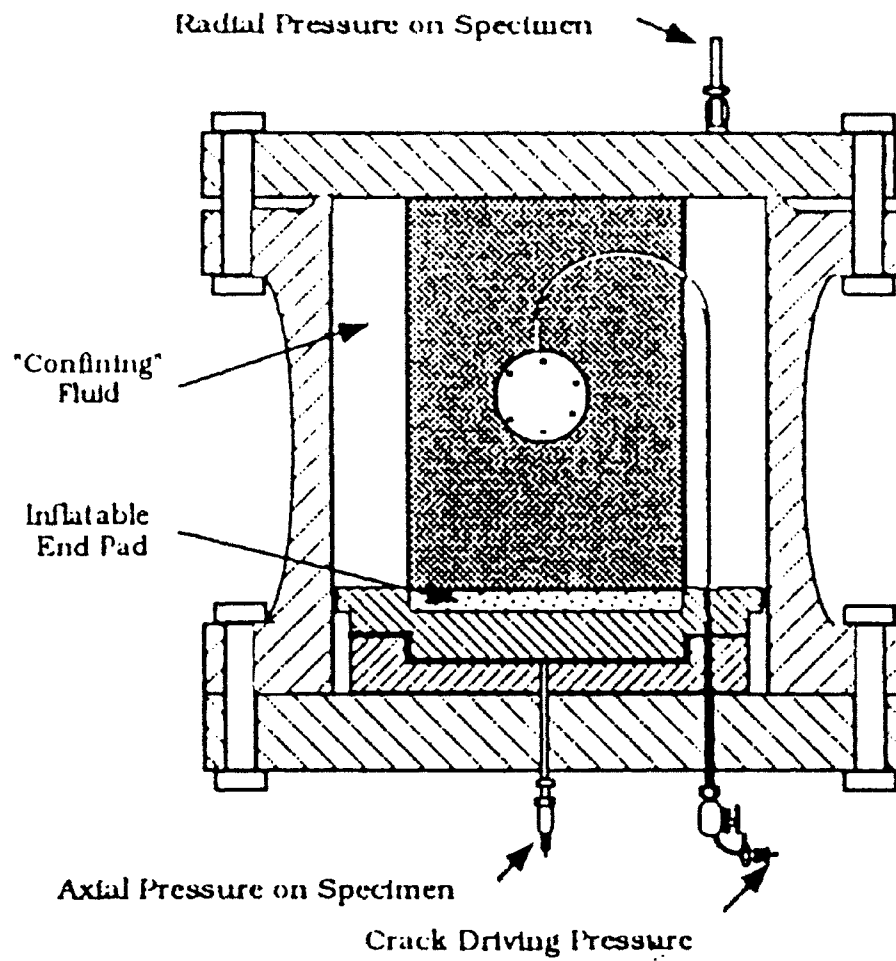


Figure 3. Hydraulic fracturing test apparatus used to grow quasi-static cracks toward cylindrical inclusions. Independent control of the axial and radial pressures permits periodic marking of the crack front.

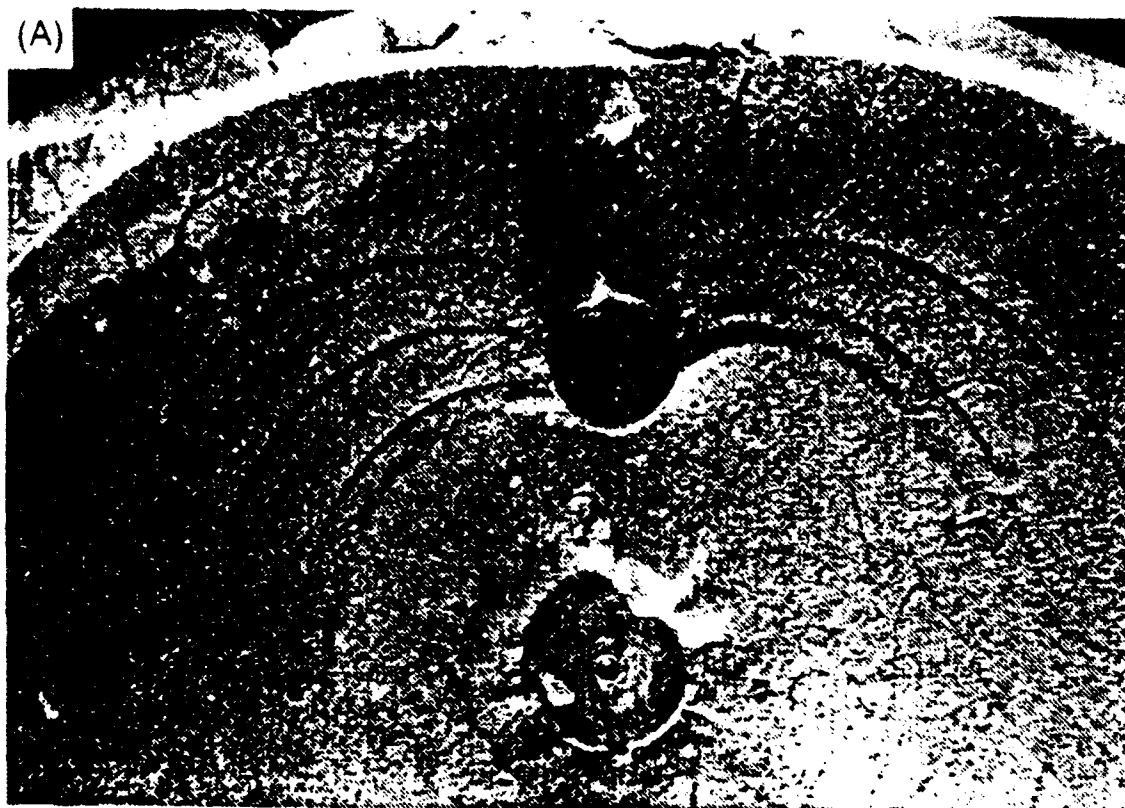


Figure 4. Representative photographs showing the local influence of a brittle inclusion on fracture propagation. The two contrast the growth patterns around a brittle fiber for a "strong" (a) and a "weak" (b) interface.

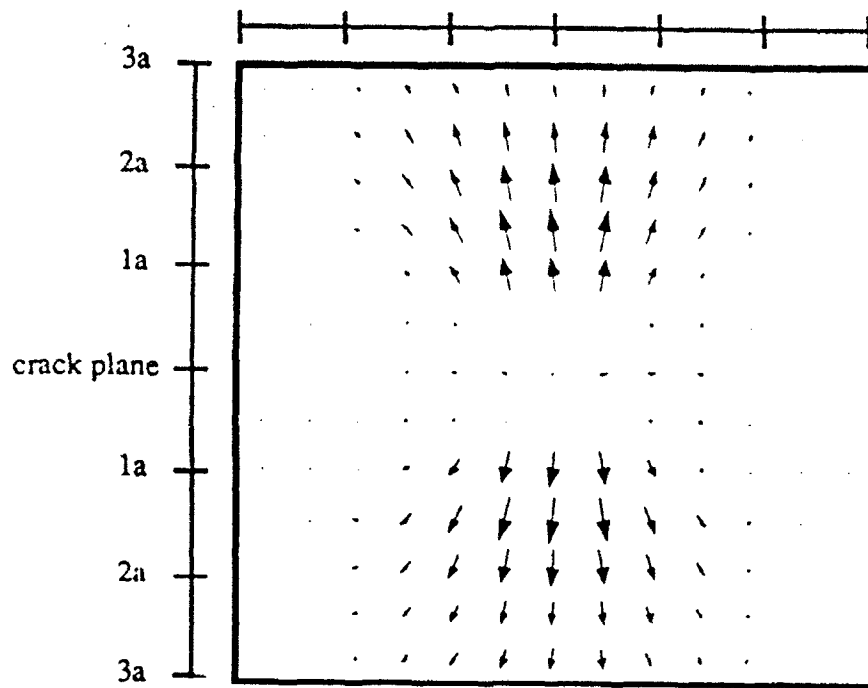


Figure 5. Vector plot showing the onset of sliding on a planar interface ahead of a pressurized circular crack.

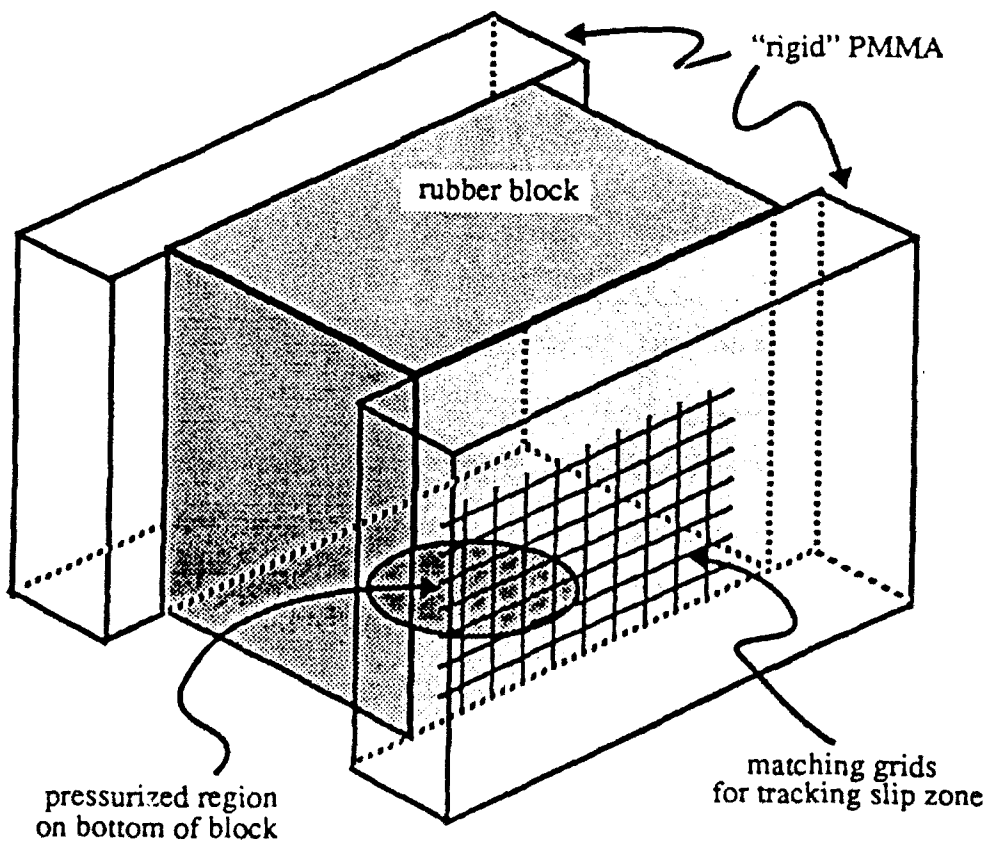


Figure 6. Schematic of ISE apparatus for direct observation of interfacial slip near a material discontinuity (crack).

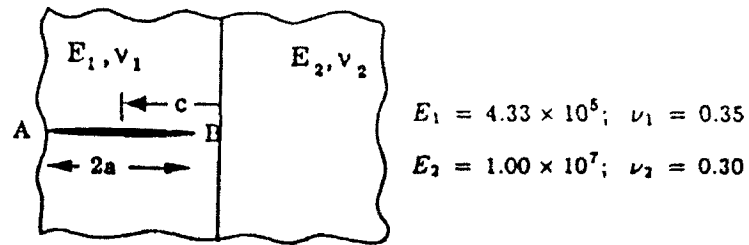


Figure 7. Fracture (under plane strain conditions) approaching a single planar bimaterial interface. See Table 1 for results.

c/a	$\left(\frac{K_I}{\sigma\sqrt{\pi a}}\right)_A$	(% Deviation) _A	$\left(\frac{K_I}{\sigma\sqrt{\pi a}}\right)_B$	(% Deviation) _B
2.0	0.9682	0.686	0.9416	0.717
1.25	0.9202	0.404	0.7887	0.625
1.15	0.9078	0.298	0.7250	1.003
1.10	0.9010	0.278	0.6787	1.693
1.00	0.8841	0.159	0.5221*	—

Table 1. Comparison of Cook and Erdogan's²⁸ plane strain solution with the 3-D surface integral results.

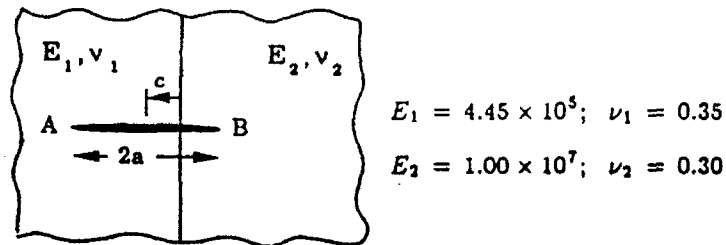


Figure 8. Fracture (under plane strain conditions) intersecting a planar bimaterial interface. See Table 2 for results.

c/a	$\left(\frac{K_I}{\sigma\sqrt{\pi a}}\right)_A$	(% Deviation) _A	$\left(\frac{K_I}{\sigma\sqrt{\pi a}}\right)_B$	(% Deviation) _B
1.0	0.8840	0.147	—	—
.75	0.8734	0.000	0.5597	-5.245
.50	0.9124	-0.642	0.7916	-1.395
.25	0.9984	-1.723	0.9524	-1.008
0.0	1.144	-2.97	1.083	-0.923
-.25	1.378	-4.149	1.194	-0.870
-.50	1.774	-5.203	1.287	-0.946
-.75	2.621	-5.304	1.364	-1.132
-1.0	—	—	1.360	0.354

Table 2. Comparison of Erdogan and Biricikoglu's²⁹ plane strain solution with the 3-D surface integral results.

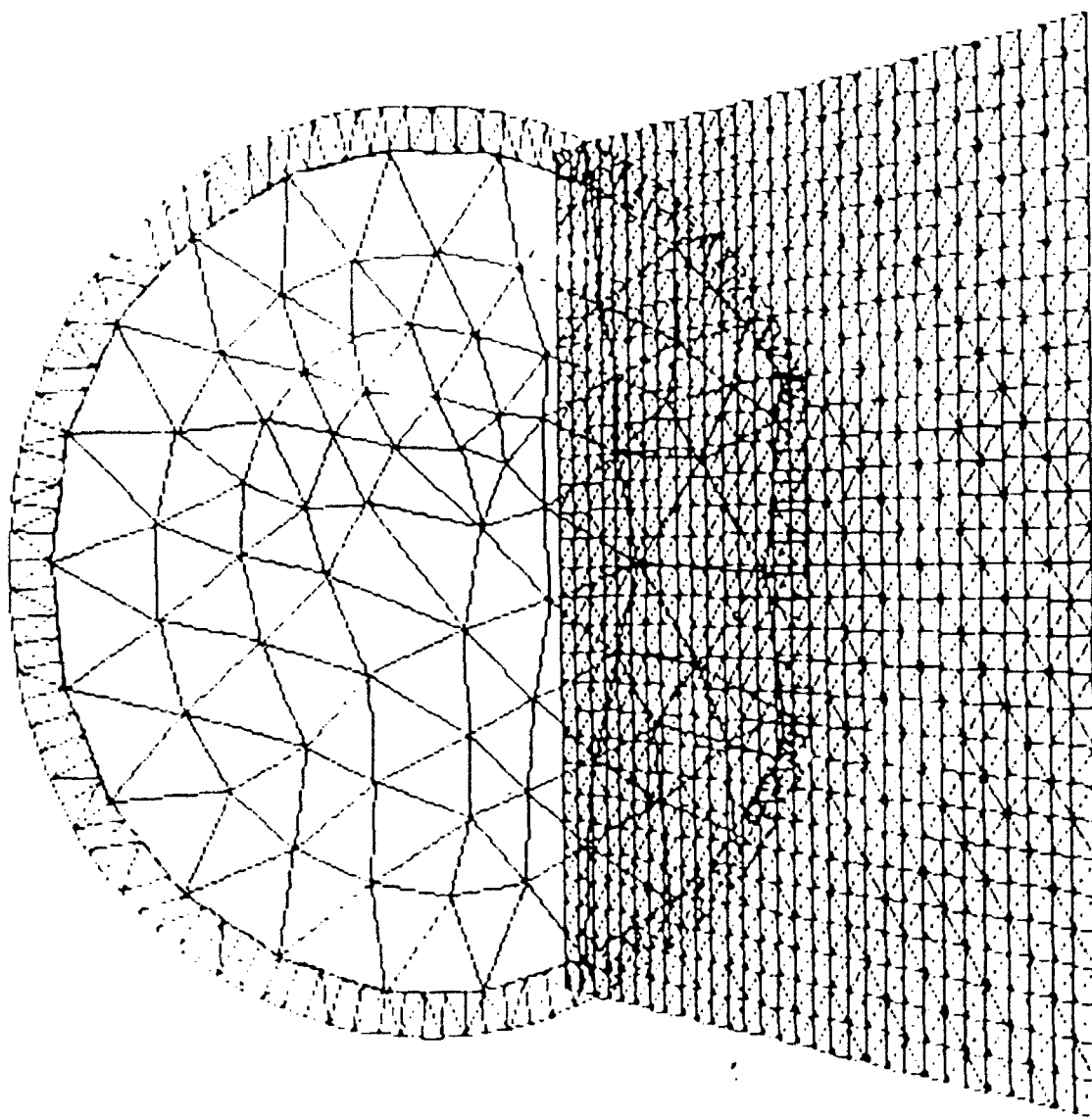


Figure 9. Snapshot from an animation showing the blunting of a fracture as it reaches a planar bimaterial interface. The fracture lies in the softer medium.

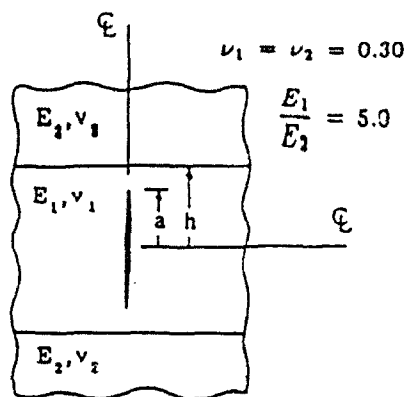


Figure 10. Fracture (under plane strain conditions) approaching two planar bimaterial interface. See Table 3 for results.

a/h	$\frac{K_I}{\sigma\sqrt{\pi a}}$	% Deviation
0.3	1.040	0.970
0.6	1.156	0.522
0.9	1.611	2.611

Table 3. Comparison of Hilton and Sih's plane strain solution with the 3-D hybrid results.

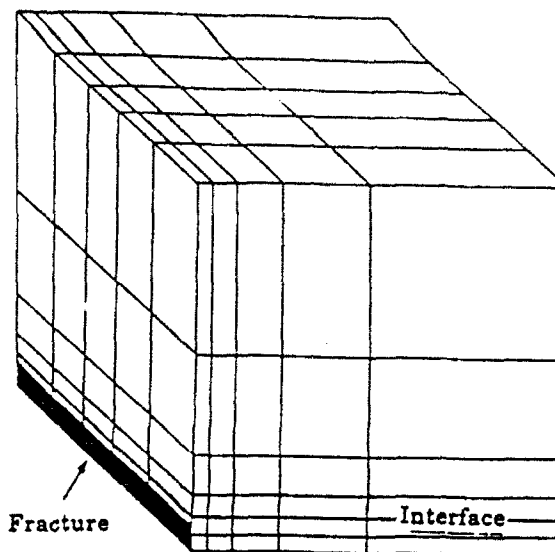


Figure 11. 1/8 symmetric hybrid model used with the double interface problem.

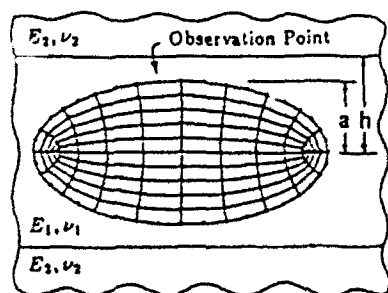


Figure 12. Elliptical fracture approaching two planar bimaterial interfaces. The fracture has been represented by its surface integral discretization.

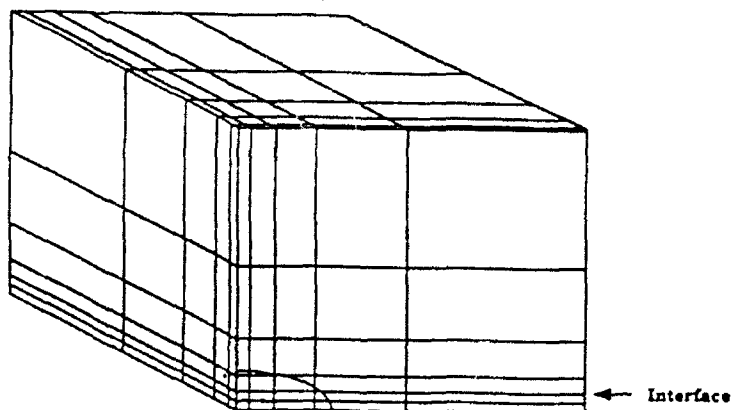


Figure 13. 1/8 symmetric model of the elliptical fracture in a tri-layered domain.

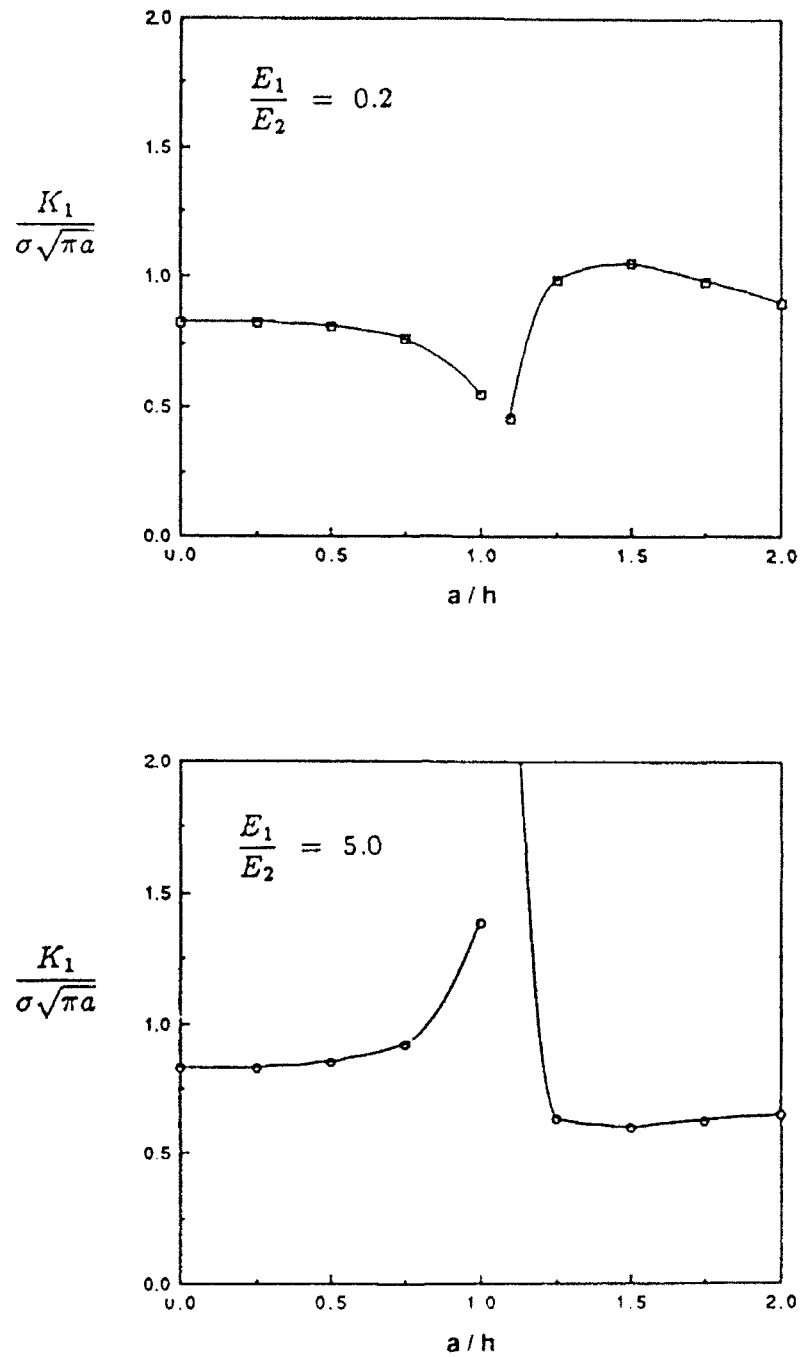


Figure 14. Dependence of K_I on the value of a/h for a 3-D elliptical fracture in a tri-layered domain. Results for two different ratios of the elastic moduli are presented. Values of K_I were recorded at the observation point indicated in Figure 12.

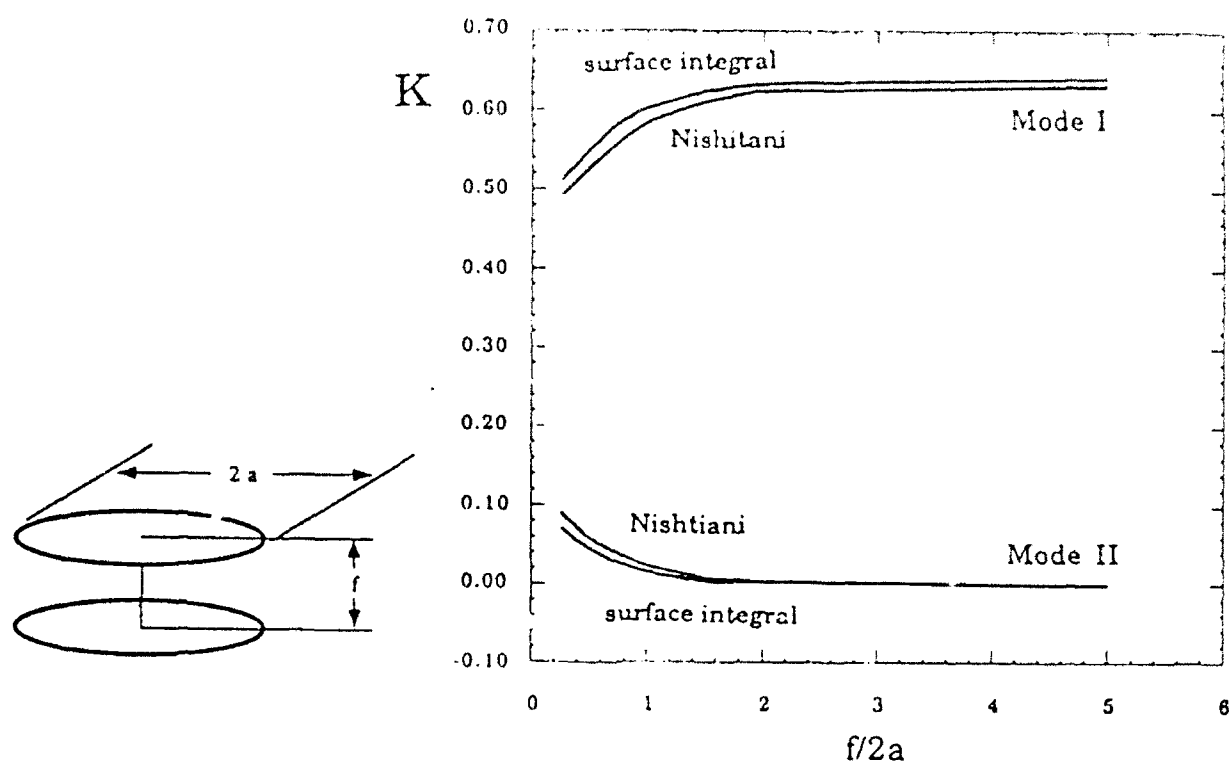


Figure 15. Variation of Mode I and Mode II stress intensity factors with distance between parallel circular cracks.

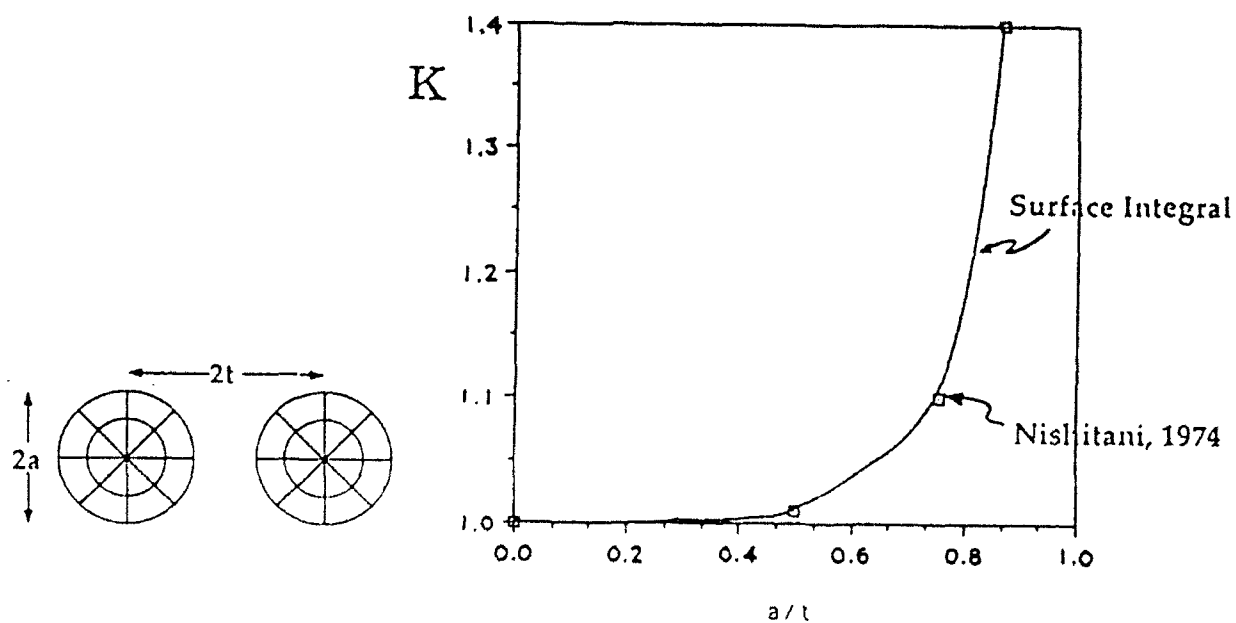
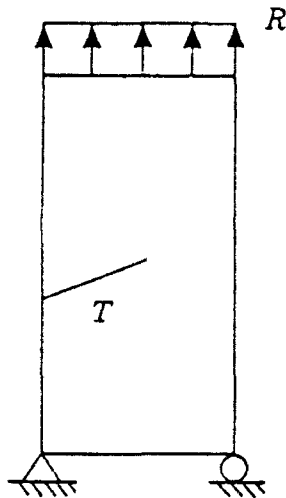


Figure 16. Variation in maximum stress intensity factor with distance between coplanar cracks.

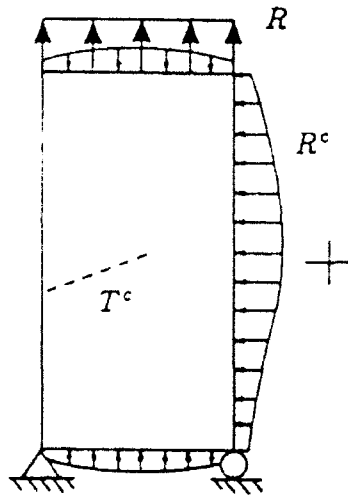
Actual Problem

Model I

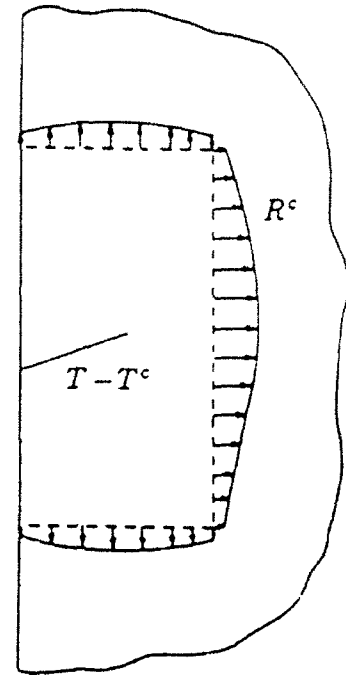
Model II



=



+



Finite Element Model of
the bounded domain (no
fracture)

Surface Integral Model of
the fracture in a semi-infinite
domain

Figure 17. Component geometries used with the hybrid method to model a surface crack in a bounded domain.

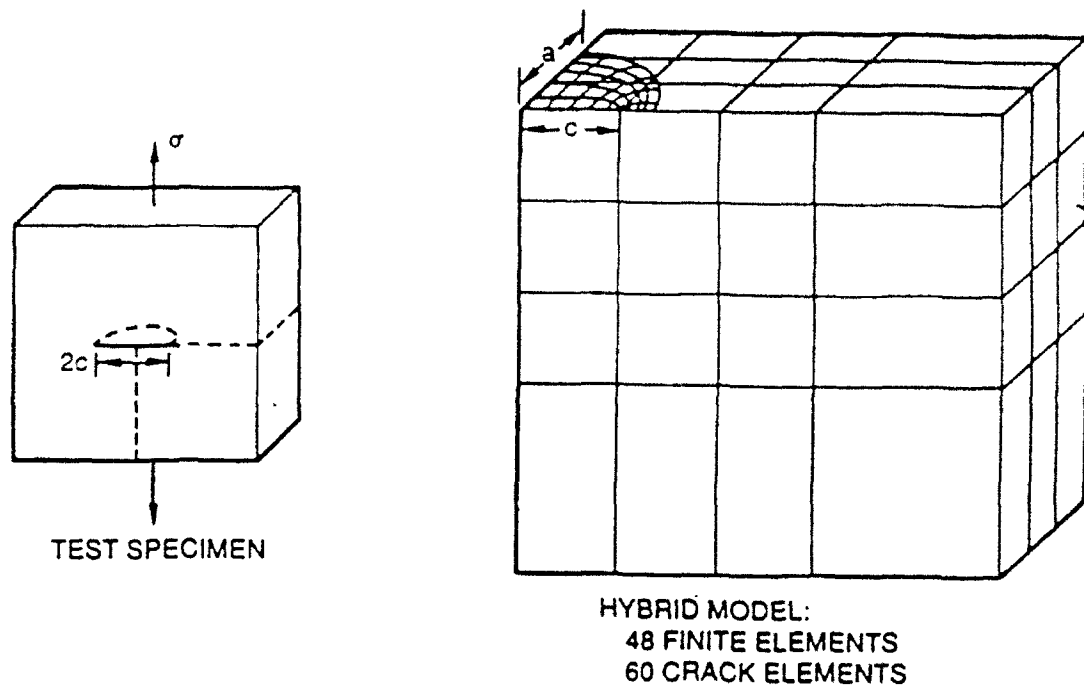


Figure 18. Specimen geometry and corresponding hybrid model used in fatigue crack growth study.

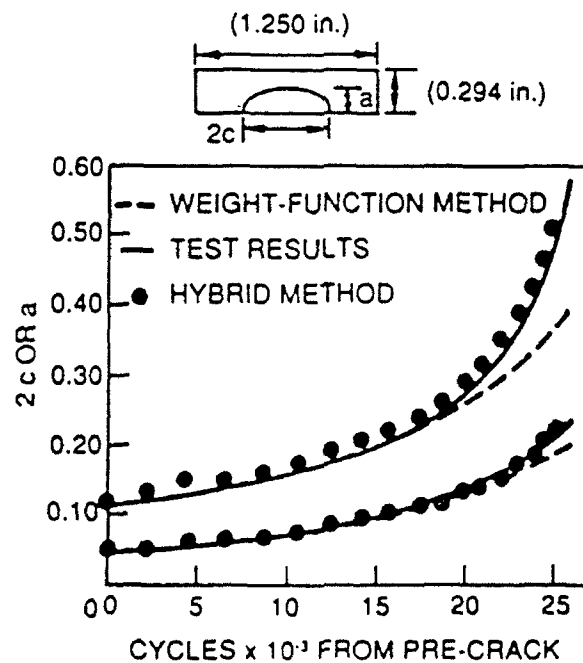


Figure 19. Comparison of SAFE and experimental results for growth of a surface crack in a thick plate.

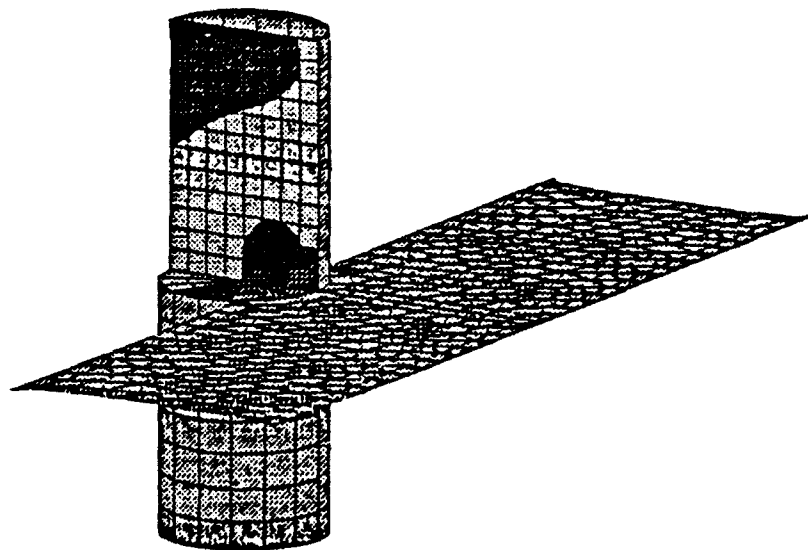


Figure 20. Snapshot of a simulation of a matrix crack moving toward and around a fiber with $\mathcal{FG}=0.1$

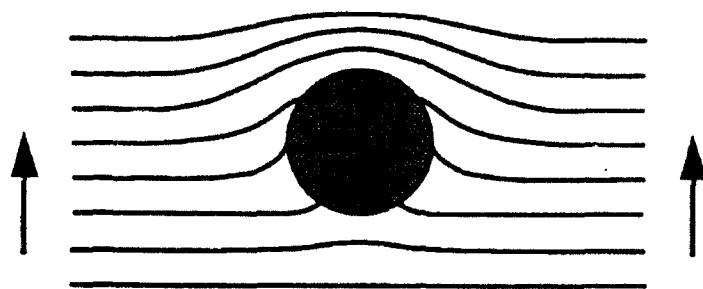


Figure 21. Crack-front profiles for a wide crack propagating past a fiber with a frictional interface, $\mathcal{FG}=0.01$. The arrows indicate direction of propagation.

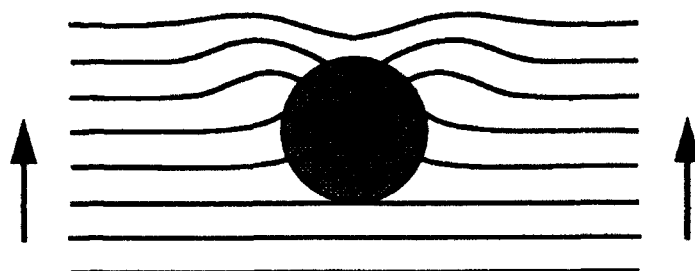


Figure 22. Crack-front profiles for a wide crack propagating past a fiber with a frictional interface, $\mathcal{FG}=0.1$. The arrows indicate direction of propagation.

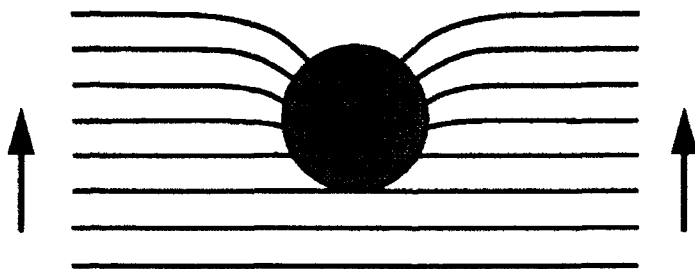


Figure 23. Crack-front profiles for a wide crack propagating past a fiber with a frictional interface, $\mathcal{FG}=1.0$. The arrows indicate direction of propagation.

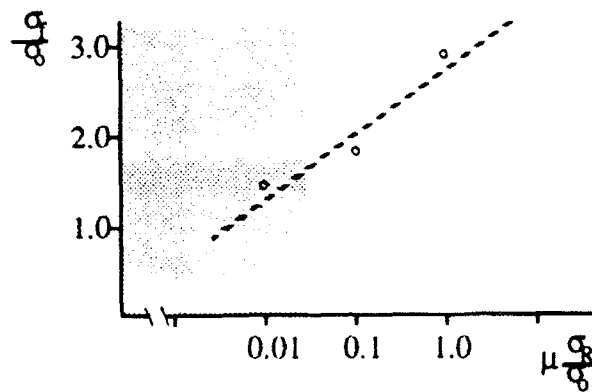


Figure 24. Design trend for optimal determination of interfacial frictional grab. The maximum local stress concentration in the fiber is presented as a function of G_{grab} for a single fiber in the reference state. The shaded region denotes values at which matrix toughening will not occur and at which there is no prospect for arresting small cracks.